



Full length article

Cross-kinks control screw dislocation strength in equiatomic bcc refractory alloys

Xinran Zhou^{a,*}, Sicong He^a, Jaime Marian^{a,b}^a Department of Materials Science and Engineering, University of California, Los Angeles, CA 90095, USA^b Department of Mechanical and Aerospace Engineering, University of California, Los Angeles, CA 90095, USA

ARTICLE INFO

Article history:

Received 27 December 2020

Revised 29 March 2021

Accepted 4 April 2021

Available online 9 April 2021

Keywords:

Multielement alloys

High entropy alloys

Screw dislocations

Kinetic Monte Carlo simulations

Strength of materials

Dislocation dynamics

ABSTRACT

Refractory multi-element alloys (RMEA) with body-centered cubic (bcc) structure have been the object of much research over the last decade due to their high potential as candidate materials for high-temperature applications. Most of these alloys display a remarkable strength at high temperatures, which cannot be explained by the standard model of bcc plasticity based on thermally-activated screw dislocation motion. Several works have pointed to chemical energy fluctuations as an essential aspect of RMEA strength that is not captured by standard models. In this work, we quantify the contribution of screw dislocations to the strength of equiatomic Nb-Ta-V alloys using a kinetic Monte Carlo model fitted to solution energetics obtained from atomistic calculations. In agreement with molecular dynamics simulations, we find that chemical energy fluctuations along the dislocation line lead to measurable concentrations of kinks in equilibrium in a wide temperature range. A fraction of these form cross-kink configurations, which are ultimately found to control screw dislocation motion and material strength. Our simulations (i) confirm that the evolution of cross kinks and self-pinning are strong contributors to the so-called 'cocktail' effect in this alloy at low temperature, and (ii) substantiate the notion that screw dislocation plasticity alone cannot explain the high temperature strength of bcc RMEA.

© 2021 The Authors. Published by Elsevier Ltd on behalf of Acta Materialia Inc.

This is an open access article under the CC BY license (<http://creativecommons.org/licenses/by/4.0/>)

1. Introduction

Since their inception in the 1990s [1,2], high entropy alloys (HEA) have attracted a great deal of attention due to a unique combination of properties seldom found in other material types [3–11]. This makes them potentially very attractive as candidate materials for a number of technological applications with harsh environments such as elevated temperatures, irradiation, or corrosion [12–15]. The basic idea behind creating alloys of this type is to combine a number of elements (typically four or more) in similar proportions to achieve solid solution phase stability through the large configurational entropy of the system. Due to the large chemical and configurational space available to create these materials, several hundred different HEA combinations now exist, each with their own distinct compositions, structure, and properties [16–18]. The large volume of research on the topic over the last decade has resulted in a fast-evolving field full of new findings, unexplained

results, and unresolved controversies. The reader is referred to the numerous reviews and monographs published over the last several years for more details [3–10,19,20]. Note that, while the term 'multicomponent' or 'multielement' alloys is sometimes preferred in the literature over 'high-entropy' alloys (particularly when the number of elemental constituents is less than five), here we use both interchangeably.

Among the different materials proposed, refractory multi-element alloys (RMEA) are a special class of alloys composed of typically four or more refractory metal elements (Nb, Mo, Ta, V, W, Cr, Hf, Zr). While compositionally complex, these systems generally crystallize into a simple body-centered cubic (bcc) phase, found to be stable up to very high temperatures [9,21–27]. RMEA display sluggish self-diffusion rates [28–31] and, similar to their pure bcc metal counterparts, suffer from a lack of ductility at low temperatures [21,32]. However, they retain high strength and ductility at high temperature, making them attractive candidates for structural applications in the power, aerospace, or nuclear sector [12–14,19,33].

While the deformation mechanisms of bcc metals and their alloys are relatively well understood, theories that explain the

* Corresponding author.

E-mail addresses: Xinranz1216104@ucla.edu (X. Zhou), jmarian@ucla.edu (J. Marian).

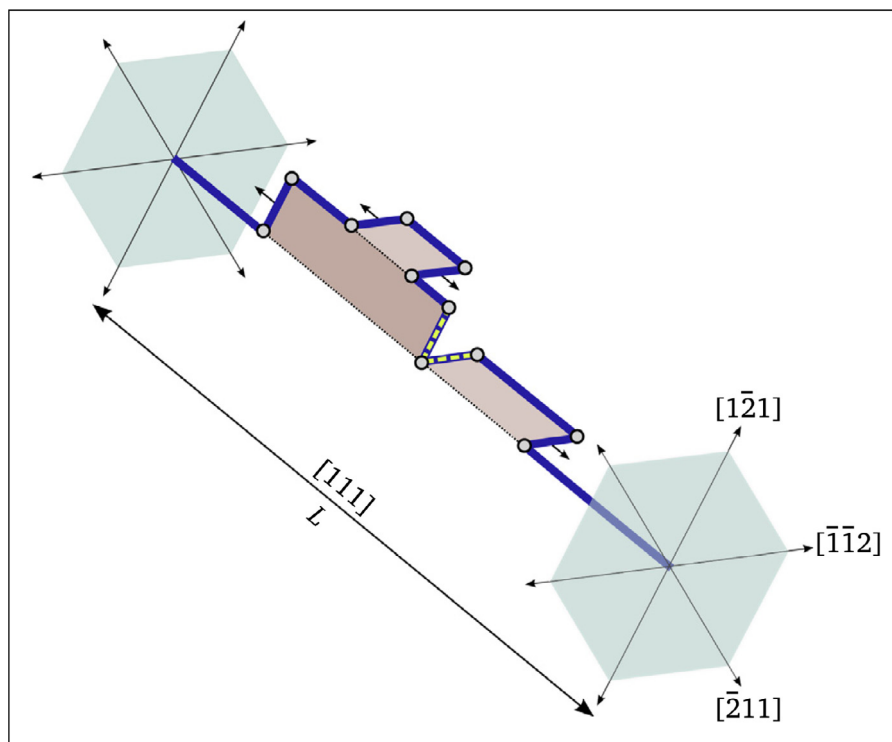


Fig. 1. Schematic depiction of an arbitrarily kinked screw dislocation line showing kink-pairs on two different $\{110\}$ planes. The arrows indicate the direction of motion of kinks under an applied stress that creates a force on the dislocation in the $[\bar{1}\bar{1}2]$ direction. The dashed segments depict a cross-kink. Shaded quadrilaterals represent the area swept by the dislocation on different glide planes when a kink pair is produced. The length of the kink step is exaggerated for ease of visualization (reproduced from ref. [39] with permission from Elsevier).

behavior observed in body-centered cubic RMEA have only recently begun to be developed [34–37]. These theories are built around the idea that each atom in the alloy can be regarded as a solute atom in an effective matrix defined by the average properties of the constituent elements. As such, every single atom in the lattice contributes to (solution) hardening, potentially resulting in a large strengthening effect (often referred to as ‘cocktail’ effect). At the same time, these local chemical fluctuations enhance the concentration of equilibrium kinks on screw dislocation lines, potentially reducing the importance of kink-pair nucleation and shifting it instead to kink lateral motion. This signifies a departure from ‘classical’ bcc metal plasticity, which is known to be controlled by the thermally-activated glide of $1/2\langle 111 \rangle$ screw dislocations on close-packed planes by way of kink-pair nucleation and propagation [38–40]. As well, phenomena connected to non-MRSS glide, such as anomalous slip, pencil glide, etc [41,42], all of which are known to occur in bcc metals, may be exacerbated in chemically-complex systems such as RMEA.

One lingering question that results from these theories, however, is whether local compositional variations can be subsumed into simple statistical distributions based on the set of solute-dislocation core interaction energies. These interaction energies can be accurately calculated using first-principles methods [35,43,44] and are indicative of the attractive or repulsive nature of the interaction between lattice atoms and dislocation cores. A collateral effect of the interactions of dislocations with lattice atoms is the potential enhanced formation of so-called *cross kinks*, i.e. collisions of kinks on different glide planes [45] that result in non-gilssile structures (see Figure 1). Aided by the existence of a large density of lattice mismatch points along the dislocation line, kinks may slow their lateral motion or become arrested, thus increasing the likelihood of kink collisions and cross-kinks. This could result in considerable self-pinning, which may also help explain the behavior of certain RMEA.

To investigate the above points and to complement existing statistical theories, in this paper we simulate the motion of screw dislocations in a discrete bcc lattice representing a multielement alloy using a kinetic Monte Carlo (kMC) model developed originally for pure and dilute bcc systems [46–48]. Specifically, we study an equiatomic Nb-V-Ta alloy to take advantage of existing interaction energy calculations [49]. While the kMC model makes use of a number of approximations, it allows us to explore the features of slip associated with three-dimensional behavior and long dislocation lines. Thus, this work is a first attempt to embed some of the complexity of the highly-random alloy into a mesoscale framework with the aim of capturing time and length scales more suitable for experiments, as compared to MD.

The paper is organized as follows. First, we provide the theoretical framework for the kinetic Monte Carlo model. This is followed by a description of the numerical implementation and modifications of the kMC simulator to adapt it to the alloy of choice. Next we present results of the strength of the alloy as a function of temperature and strain rate. We finalize the paper with a discussion of the results and the conclusions.

2. Kinetic Monte Carlo model of screw dislocation motion in a multielement alloy

2.1. Pure metal formulation

As discussed above, plasticity in bcc metals is governed by the motion of screw dislocations on close-packed planes. Generally, this motion is understood to occur over a periodic energy landscape known as the Peierls potential U_p . U_p is typically quite stiff, resulting in high critical (Peierls) stresses, τ_p , [50,51], and at low-to-medium homologous temperatures slip proceeds via thermally-activated nucleation of steps on the dislocation line, known as *kink pairs*, and their subsequent sideward relaxation. Kink-pair nucle-

ation is a rare event, i.e., one that occurs with a low probability over the scale of atomic vibrations. Thus, methods with high temporal resolution such as molecular dynamics are not suitable for simulating the long-term kinetics of the system. Instead, kinetic Monte Carlo evolves the system efficiently through a sequence of thermalized states connected by transitions that define ‘events’. In kMC, one simply specifies the transition rates of different events, which represent the probability per unit time that they will occur, and then time evolves in discrete increments. With this approach, the atomistic features of the dislocation core, such as atomic vibrations and local distortions, are not directly resolved, but their effective kinetic behavior is condensed into physical transition rates that can be characterized atomistically. This is what allows us to explore mesoscopic length and time scales. Adaptations of the kMC method to simulate thermally-activated screw dislocation motion have been successfully applied to pure bcc crystals [39,52] and dilute alloys [47,48,53].

The kink-pair nucleation rate for a segment i of length ℓ_i (note that the total screw length line L is conserved: $L = \sum_i \ell_i$) is expressed as a function of stress and temperature as [39]:

$$\omega_{kp_i}(\tau_i, T) = \nu_0 \frac{\ell_i - w}{b} \exp\left(-\frac{\Delta H_{kp}(\tau_i)}{kT}\right) \quad (1)$$

where τ_i and T are the local resolved shear stress and the temperature, respectively, ν_0 is an attempt frequency, ℓ_i is the dislocation segment length, w is the total width extent of a kink pair, b is the Burgers vector’s modulus, and ΔH_{kp} is the kink-pair activation enthalpy. ℓ_i is itself delimited by kinks on both sides, while w includes the distance between kinks, λ_{kp} , at the point of nucleation plus the spread, a , of each kink, i.e., $w = \lambda_{kp} + 2a$. The above expression is only defined for positive nucleation lengths, $(\ell_i - w) > 0$, with segments shorter than w being discarded for the purposes of calculating ω_{kp} . In pure bcc metals, a common expression for ΔH_{kp} is the one proposed by Kocks et al. [54]:

$$\Delta H_{kp}(\tau) = \Delta H_0 \left(1 - \left(\frac{\tau}{\tau_p}\right)^p\right)^q$$

where ΔH_0 is the sum of the energies of two infinitely-separated opposite kinks, and p and q are fitting parameters. We have extended this expression to account for non-Schmid effects on dislocation glide in past works [39,40,55], and dilute solid solution interactions [47,48]. For their part, kinks move a distance $\delta y = v_k \delta t \pm \xi \sqrt{2D_k} \delta t$ during a given time increment δt , where v_k and D_k are the kink velocity and diffusivity, respectively, and ξ is a uniform random number. v_k and D_k represent mechanically-driven (stress-dependent) and diffusive (stress-independent) contributions to the kink motion. Generally, δt is chosen as the ‘waiting’ time for kink pair nucleation, such that the position of existing kinks (if any) is updated prior to the next nucleation event. To avoid unphysically long kink propagation events, δy is typically capped at some distance on the order of w . Due to the finite spread, a , of individual kinks, kink pairs are considered to have a trapezoidal shape, rather than a rectangular one, for the purpose of calculating elastic stresses. However, during visualization kinks are represented as straight (i.e., pure edge) segments for simplicity.

Kink segments are identified by their non-screw character, i.e., when $|\vec{\ell} \cdot \vec{s}| < 1$, where $\vec{\ell}$ and $\vec{s} = \vec{b}/b$ are the line tangent and the slip direction, respectively. Kinks are tracked in space and time throughout the simulation by monitoring their vectors $\vec{\ell}$, \vec{s} (constant), and $\vec{n} = \vec{s} \times \vec{\ell}$ (representing the glide plane). Two kinks mutually annihilate if (i) they have opposite line directions (projected along the glide direction), (ii) they share a common \vec{n} vector, and (iii) they are within an interaction distance a of one another. When all three conditions are met, the two kink segments are eliminated and the screw dislocation line is reconnected on the Peierls valley common to both.

The underlying topology supporting dislocation and kink segments is a discrete bcc lattice oriented along the [111] direction, as shown in Figure 1. The figure shows a schematic depiction of a dislocation of total length L containing several kink pairs and a cross-kink (dashed segments). The crystal model thus includes all possible lattice point locations in case they are needed for specific calculations, which is the case in multi-element systems. Simulations can be done with periodic boundary conditions or with finite-sized lines. Unless otherwise noted, here we use finite dislocation lines of length $L = 500b$ pinned at both ends to mimic the operation of a Frank-Read source in the material. Shear stress is applied such that the $(1\bar{1}0)$ plane is always the maximum resolved shear stress (MRSS) plane (cf. Fig. 1).

2.2. Strain rate-controlled simulations

The dependence of the applied stress with strain rate (in tensor form) can be written as:

$$\sigma(t) = C(\dot{\epsilon}_0 t - \epsilon^P(t)) \quad (2)$$

where C is the elasticity matrix, $\dot{\epsilon}_0$ is the prescribed strain rate tensor, and ϵ^P is the accumulated plastic strain tensor. Assuming small plastic deformations, the tensor ϵ^P evolves as:

$$\epsilon^P(t^{m+1}) = \epsilon^P(t^m) + \delta \epsilon^P(t^{m+1}) \quad (3)$$

$$\delta \epsilon^P(t) = \left(\frac{\vec{s} \otimes \vec{n} + \vec{n} \otimes \vec{s}}{2}\right) \left(\frac{b}{L}\right) \rho_d \delta A(t) \quad (4)$$

with ρ_d being the dislocation density (constant), L the total dislocation line length, and δA the area swept by the dislocation during a given $\delta t = t^{m+1} - t^m$ time interval (between kMC steps m and $m+1$). The Schmid tensor $1/2(\vec{s} \otimes \vec{n} + \vec{n} \otimes \vec{s})$ is used to obtain the appropriate projection of δA .

The only component of $\dot{\epsilon}_0$ that produces a nonzero resolved shear stress in the present geometry is a shear strain rate of the xz type. Consequently, the relevant applied stress component is obtained as:

$$\tau_{xz}(t) = 2\mu((\dot{\epsilon}_0)_{xz} t - \epsilon_{xz}^P) \quad (5)$$

and, accordingly, $\epsilon_{xz}^P(t^{m+1}) = \epsilon_{xz}^P(t^m) + \delta \epsilon_{xz}^P(t^{m+1})$. Thus, in the present setup, the plastic strain update is reduced to:

$$\delta \epsilon_{xz}^P = \frac{\rho_d n_y b \delta A}{2L} \quad (6)$$

where n_y is the component of the plane normal resolved along the glide direction. δA is calculated depending on whether the event is a kink pair nucleation event, or the propagation of a kink. In each case, the area swept at a given time is written as:

$$\delta A = \begin{cases} hw, & \text{kink pair nucleation} \\ h\delta y, & \text{kink displacement} \end{cases} \quad (7)$$

Thus, in this approach, the stress τ_{xz} is a time-varying output that is added to the local elastic stresses everywhere in the simulation volume. In the forthcoming graphs and plots, we simply refer to this stress as ‘ τ ’.

As eqs. (5) and eq. (6) indicate, the value of the shear stress depends parametrically on the dislocation density. However, this is a weak dependence as we have carefully confirmed in independent tests¹. Nonetheless, ρ_d has a quantitative impact on the value of τ and all simulation results should be interpreted in the context of the dislocation density considered.

¹ By way of example, in a set of strain-rate-controlled simulations at 10^{-3} s^{-1} in pure W at 300 K where ρ_d was varied between 10^{10} and 10^{14} m^{-2} , τ was seen to decrease by 30%, from 800 to 650 MPa.

2.3. Environment-dependent kink pair nucleation and kink propagation rates

As explained above, the model employed to describe a multicomponent alloy involves the superposition of an effective substrate (often referred to as the ‘average’ alloy) whose properties are taken as the compositional average of each of the individual element properties, and a set of lattice atoms representative of the chemical composition of the alloy. As such, eq. (1) must be modified to capture this new physical system and its effect on the dislocation kinetics. The principal modifications to the model are listed below:

1. Segment-segment elastic interactions are considered at the substrate level using the elastic constants of the *average* alloy.
2. We assume that all interactions between dislocation segments and lattice atoms are additive and pairwise, i.e., their interaction energy depends only on the chemical identity of the atom in question, regardless of the broader local chemical environment [35,56].
3. The kink-pair nucleation enthalpy is written as a sum that includes ‘solute’ interaction energies:

$$\Delta H_{kp}(\tau_{RSS}) = (\Delta H_0 + \Delta E_{x \rightarrow x+h}^{int}) \left(1 - \left(\frac{\tau_{RSS}}{\tau_p} \right)^p \right)^q \quad (8)$$

where ΔH_0 is the formation energy of a pair of isolated complementary kinks in the average alloy (average across all constituent elements), $\Delta E_{x \rightarrow x+h}^{int}$ is the change of ‘chemical’ energy across one Peierls valley (i.e. between x and $x+h$) on a given dislocation segment i (with length ℓ_i), τ_p is the Peierls stress of the average alloy, and p and q are fitting parameters.

4. In alloys, kink motion is itself thermally activated and thus treated also as an Arrhenius process with activation energy equal to $\Delta E_{y \rightarrow y+b}^{int}$, i.e. the excess energy that results when kinks move an amount b along the y (i.e., [111]) direction:

$$\omega_k(\tau_{RSS}; T) = \nu_1 \exp \left(- \frac{\Delta E_{y \rightarrow y+b}^{int} - \tau_{RSS} \Delta \Omega_k}{kT} \right) \quad (9)$$

where ν_1 is an attempt frequency not necessarily equal to ν_0 . Defined in this fashion, $\omega_k(T)$ represents the hopping rate of a kink segment going from a position y to another $y+b$. Note that, as defined, $\Delta E_{y \rightarrow y+b}^{int}$ may be negative (and, often, small, such that $\Delta E_{y \rightarrow y+b}^{int} \ll kT$), in which case the advancement (or recoil) of the kink by a distance b is executed without needing to compute its thermally-activated rate. As defined, eq. (9) defines a unidimensional hopping rate and thus replaces D_k (introduced in Sec. 2.1) for kink propagation. With this, (7) is modified to $\delta A = hb$.

Equations (8) and (9) are then sampled according to the kMC algorithm for any available dislocation segment with length greater than w and for all existing kinks. In these two equations, the dependence on stress is through the resolved shear stress (RSS), τ_{RSS} , which is a scalar quantity that represents the local projection of the total stress tensor σ on the glide plane of the dislocation, including non-Schmid effects if appropriate. σ contains contributions from the externally applied stress and from the different dislocation segment stress fields, as described in refs. [39,57]. Our model can efficiently calculate long-range stresses originating from dislocation segments, both using isotropic and anisotropic elasticity theory [57,58].

2.3.1. Calculation of interaction energies for kink-pair nucleation

$\Delta E_{x \rightarrow x+h}^{int}$ and $\Delta E_{y \rightarrow y+b}^{int}$ represent excess energies in translating segments of the dislocation from one location to another. As such, they are calculated for a specific spatial arrangement of lattice

Table 1

Dislocation core solute-interaction energies (solute in average-atom matrix). Site numbers are given in relation to the diagram on the right column (adapted from ref. [49]). All energies in eV (from ref. [49]). Negative values indicate attraction.

Site	e_{Nb}^{int}	e_{Ta}^{int}	e_V^{int}	Diagram
1	-0.0121	0.013	-0.0043	
2	-0.0063	0.0164	-0.0137	
3	0.0113	0.0028	-0.0147	
4	0.0016	0.0035	-0.0047	
5	0.006	0	-0.0059	
6	0.0036	0.0008	-0.0041	

atoms, which must reflect the chemical complexity of the alloy at hand. In our case, we start from a pre-generated hexagonal prism with fixed size that does not change throughout the simulation. While the size of the prism is arbitrary, here we work with environments sufficiently large to enclose lattice atoms that are 6th-nearest neighbors to the dislocation core (atoms with the label ‘6’ in Table 1). These prisms are populated with Nb, Ta, and V atoms by random sampling the compositional proportions in the alloy (33.3% for each chemical species in our case)². Figure 2 shows the minimum prism size that captures all the non-MRSS {110} glide planes available to the dislocation segment for the calculation of the corresponding rates. In our case, we use sizes corresponding to a distance of 20 Peierls valleys (20h) from the original dislocation position. These contain in excess of 630,000 atoms for $L = 500b$. For line relaxations we use $L = 5000b$ and 12h, which contain a total of 455,000 lattice points. Each lattice site within the prism is assigned a chemical element with a probability equal to the relative alloy composition and the total interaction energy is computed as:

$$\Delta E_{x \rightarrow x+h}^{int} = \sum_j q_j e_j^{int} \Big|_{x+h} - \sum_i q_i e_i^{int} \Big|_x \quad (10)$$

where e_j^{int} are the solute (of type j) interaction energies and q_j is the number of solutes of type j surrounding the dislocation core along that segment. Note that $\Delta E_{x \rightarrow x+h}^{int}$ may be positive or negative, indicating a favorable or unfavorable effect on kink-pair nucleation, respectively. To account for correlated transitions, both forward and backward nucleation rates are considered for each viable glide plane.

2.3.2. Interaction energies for kink-pair propagation events

Likewise, $\Delta E_{y \rightarrow y+b}^{int}$ is obtained as the excess energy resulting from the sideward translation of a kink along the [111] direction, from position y to $y+b$, i.e.:

$$\Delta E_{y \rightarrow y+b}^{int} = \sum_k \left(e_i^{int} \Big|_{y+b} \mp e_i^{int} \Big|_y \right) \quad (11)$$

The kink interaction energies are calculated over the entire length of the kink spread a . The relevant configuration is illustrated in Fig. 2 (bottom) as a shaded area encompassing 12 slices of width b represented by the subindex i in eq. (11). For ease of visualization, only the atoms surrounding the initial and final Peierls valleys are shown. Here too, we calculate rates for forward and backward jumps to account for correlated motion (hence the \pm sign). The energies for both types of jumps are obtained by considering the extra atoms inside slices of width b to the left and to the right of the kink, such that a kink spread of $12b$ is always maintained. Note that, for trapezoidal kinks (with fixed dislocation character), the interaction energy change is given only by the relative energy difference between the two slices at the two ends of the kink. Stress

² Note that a ‘numerically’ random system does not necessarily correspond to thermalized RMEA lattices, as discussed in Sec. 4.2.

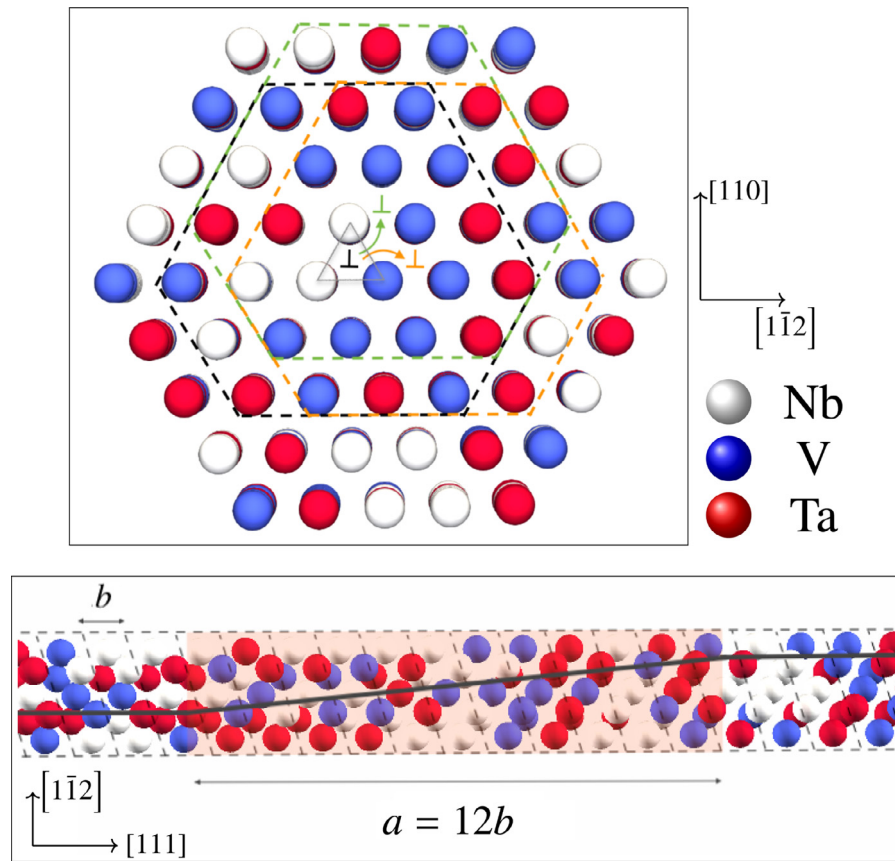


Fig. 2. Minimal atomic environment around a dislocation line required to calculate kink event rates as described in Sec. 2.3.1. The top image is a view of the dislocation core along the $[111]$ direction, showing two possible transitions to next Peierls valleys on different $\{110\}$ planes. The dashed polygons represent the maximum extent of dislocation-atom interactions as indicated in Table 1. The bottom image represents the spread of a single kink along the $[111]$ direction with the shaded area indicating the region over which the interaction energy in eq. (11) is calculated. For clarity, only atoms immediately surrounding the two adjacent Peierls valleys are shown.

Table 2

Material constants for the individual constituent elements of the equiatomic NbTaV alloy. From refs. [59,60].

Symbol	a_0 [Å]	μ [GPa]	ν	τ_p [GPa]	ΔH_0 [eV]
V	3.00	47	0.37	1.20	0.89
Nb	3.32	38	0.40	0.89	1.28
Ta	3.31	69	0.34	1.03	1.17
'average'	3.21	51	0.37	1.04	1.11

Table 3

Additional material parameters for the 'average' material.

Symbol	Value	Units
a	12	b
λ_{kp}	12	b
p	0.83	-
q	1.40	-
ρ_d	1.4×10^{14}	m^{-2}

biases this directionality by way of a suitable activation volume ($\Delta\Omega_k$ in eq. (9)). Here we take $\Delta\Omega_k$ to be the deviation of the local atomic volume in the lattice with respect to the atomic volume of the average alloy, i.e.:

$$\Delta\Omega_k = \frac{1}{3} \sum_{\alpha} \Delta\Omega_{\alpha}, \quad \Delta\Omega_{\alpha} = \frac{a_0^3|_{\alpha} - a_0^3|_{\text{avg}}}{2}, \quad \alpha = \text{'Nb'}, \text{'Ta'}, \text{'V'}$$

with all the lattice parameters a_0 given in Table 2. Contrary to eq. (10), $\Delta E_{y \rightarrow y \pm b}^{\text{int}}$ is calculated only for the glide plane on which the kink in question lies. Similarly, however, it can be positive or negative, indicating attraction towards the next atomic position or repulsion from it.

The computed values for all the e^{int} for the Nb-V-Ta alloy in relation to the dislocation core are given in Table 1. In this work, it is assumed that kinks are segments close to the screw orientation (based on values of $a = 12b$) and thus we use the same interaction energies calculated for screw cores.

Values for the average alloy are given in Table 2 as averages from the known values of Nb, Ta, and V.

Screw dislocation-specific properties, such as the single kink spread a , and the coefficients p and q have been obtained using a line tension model using the elastic constants for the average alloy, as demonstrated in He et al. [61]. Those constants, together with the rest of the relevant parameters are given in Table 3.

To illustrate the differences between using eq. (1) with a fixed value of ΔH_0 (for the average alloy) and when ΔH_0 is given by eq. (8) (multicomponent system), in Figure 3 we plot the distribution of time steps sampled over 10 ns of simulation for the average material and for the equiatomic Nb-V-Ta alloy. These time steps, δt , were obtained as the inverse of ω_{kp} yielded by eq. (1) for dislocation lines with a length of $100b$, at 300 K, and 200 MPa of applied stress.

As the figure shows, the chemical spatial heterogeneity in the alloy leads to a broadened δt spectrum compared to the average material, which has all its values within a narrow interval near 10^{-4} s. We emphasize that these simulations have been performed for numerical evaluation only, and have little physical relevance *per se*.

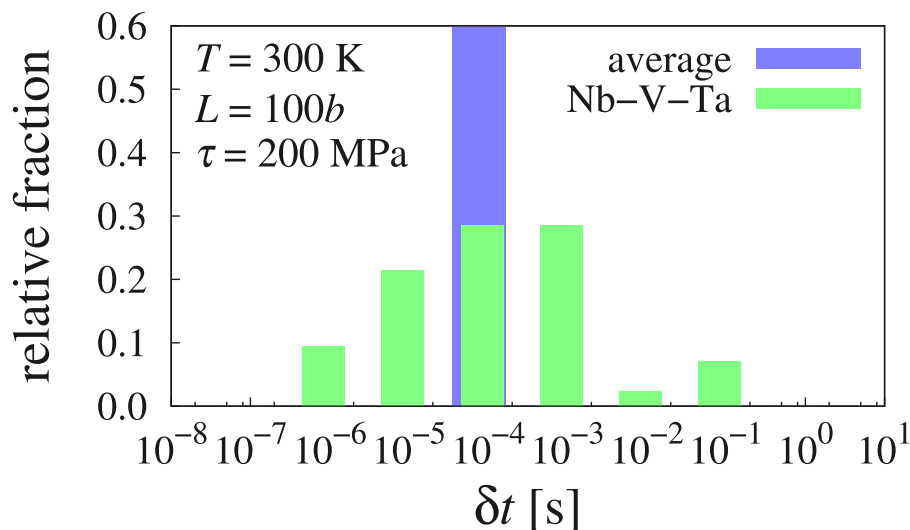


Fig. 3. Time step distributions for the average material and the equiatomic Nb-V-Ta alloy for 10 ns of simulations at 300 K and an applied stress of 200 MPa. Compared to the (uniform) average alloy, a broadened distribution is obtained for the multielement alloy.

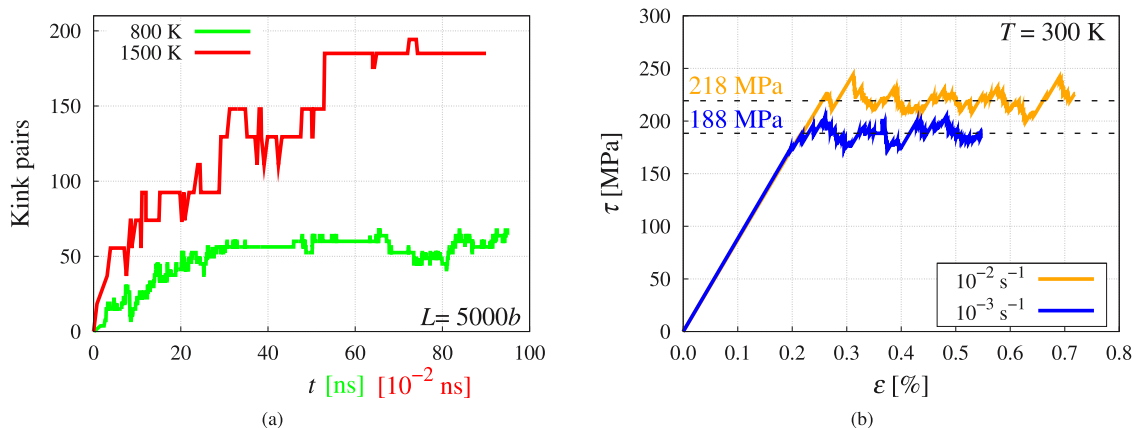


Fig. 4. (a) Time evolution of the number of kink pairs during stress-free relaxation of initially-straight dislocation lines of length $5000b$. (b) Time-dependent stress-time curves at 300 K for strain rates of $\dot{\epsilon}_0 = 10^{-3}$ and 10^{-2} s^{-1} . Dashed lines indicate the average stress values extracted from the curves. The x -axis is expressed as strain $\epsilon = \dot{\epsilon}_0 t$ to allow for comparison of both graphs on the same scale.

3. Results

3.1. Stress-free dislocation line relaxations

A recent series of atomistic simulations has confirmed that the ground state of screw dislocations in a number of multielement alloys displays an intrinsically rough structure [35,62–64] not found in simulations of pure metals or dilute alloys [39,47,48]. This is important because dislocation lines with a high intrinsic density of kinks could be potentially activated without kink-pair nucleation, which may significantly lower the effective activation stress. However, a direct consequence of this ‘roughening’ is an enhanced probability for the formation of cross-kinks, which have been linked to self-pinning as an extra contribution to dislocation hardening and alloy strength [48,65]. Within our kMC method, all of these processes can be simulated concurrently so that we can study their relative importance in a wide parametric space.

First we carry out simulations of thermal relaxation of initially-straight dislocation lines to calculate the density of kink pairs in equilibrium n_{eq} . For this analysis, lines of length $5000b$ with periodic boundary conditions were used. Steady state is reached when the number of kink pairs converges in time at a given temperature, as shown in Figure 4a. Steady state is then defined in a numerical

sense, not in a strictly thermodynamic one. Nevertheless, kink-pair numbers and total energy are directly correlated by the underlying energy model in kMC. Results for n_{eq} are shown in Figure 5 with two characteristic snapshots shown in Figure 6. Two temperature regimes can be clearly distinguished in the figure. At low T (blue markers), the data points are best fit by the Arrhenius expression $n_{\text{eq}} = 2.5 \times 10^{-3} \exp(-0.02/kT)$, i.e., with an activation energy of 0.02 eV, while at high temperatures (black dots), the best fit is given by $n_{\text{eq}} = 1.5 \times 10^{-1} \exp(-0.20/kT)$ (in units of b^{-1}). Error bars are representative of the standard deviation obtained from 15 independent simulations at each temperature.

Because n_{eq} represents the equilibrium steady-state concentration of kink pairs as a function of temperature, these energies have the meaning of average kink-pair potential energies, \bar{E}_{kp} . While it cannot be said that they are equivalent to ensemble averages in the thermodynamic sense (i.e., internal energies, see comment about convergence above), we believe that these energies accurately reflect the cost of forming a kink pair in the real alloy.

Snapshots of two resulting line configurations in steady state at 1000 and 1500 K are shown in Figs. 6a and 6b, respectively. The lines relax to their equilibrium structures consisting of multiply-kinked segments on several different glide planes. Cross-kinks can be seen to form spontaneously in the absence of any applied stress

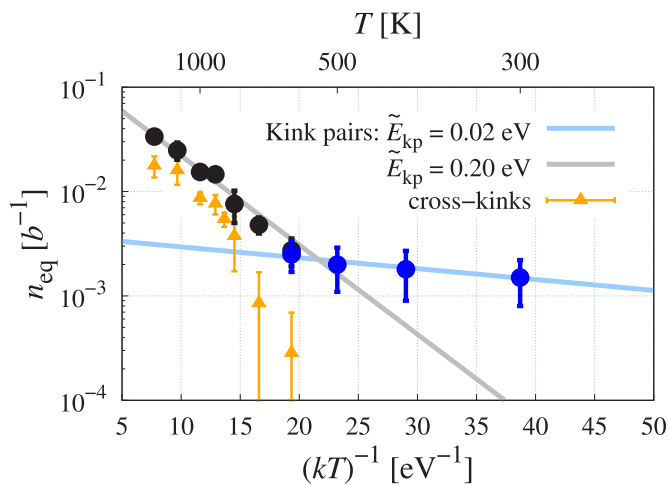


Fig. 5. Equilibrium concentration of kink pairs per unit length in Burgers vector units, n_{eq} as a function of (inverse) temperature for 5000b-long segments in the Nb-V-Ta alloy. Two regimes can be clearly appreciated, each characterized by Arrhenius fits with energies of 0.02 and 0.20 eV at low and high temperatures, respectively. Orange dots represent the equilibrium concentration of cross-kinks as a function of T . Error bars are representative of the standard variation obtained from 15 independent simulations at each temperature.

(note that elastic stresses due to kinks and screw segments exist even without applied stresses).

Further analysis of the conditions at high and low temperatures indicates that the distinctive feature separating the two regimes is indeed the presence of cross-kinks. Analysis of the concentration of cross-kinks (which is a subset of the total concentration of kinks/kink pairs), plotted as orange dots in Fig. 5, confirms that it agrees well with the variation of n_{eq} with T at high temperatures.

An independent Arrhenius fit to the cross-kink data points in the figure yields an energy of 0.37 eV. Thus, at high temperatures, $\tilde{E}_{kp}=0.20$ eV reflects a coexistence of kink pairs with $\tilde{E}_{kp}=0.02$ eV and cross-kinks with $\tilde{E}_{ck}=0.37$ eV. At temperatures below 600 K, the thermal concentration of kinks is not sufficiently large to support a measurable concentration of cross-kinks.

3.2. Strain rate sensitivity and temperature dependence of alloy strength

Next we investigate the temperature and strain-rate dependence of the alloy strength using the steady-state line configurations obtained in the previous section as the starting structures. Following the procedure discussed in Sec. 2.2, we prescribe the strain rate and measure the average stress of the system. Figure 4b shows the time-dependent response of the shear stress at two illustrative strain rates and $T = 300$ K. A crucial aspect of these simulations is to use the structures obtained in Sec. 3.1 to initialize the RMEA system, which is thus seeded with kinks/kink pairs/cross-kinks from the outset. The average stresses as a function of $\dot{\epsilon}_0$ at room temperature are shown in Figure 7 for the elementary elements Nb, Ta, and V, the average alloy, and the Nb-Ta-V alloy. Remarkably, the Nb-Ta-V system displays a higher strength at all strain rates than the rest of the materials considered (this is what has come to be known as ‘cocktail’ effect [66,67]). The reason behind this relative high strength of these complex alloys at room temperature is again found in the dynamic behavior of the dislocation, which is governed not by kink-pair nucleation but by kink propagation and the formation and dissolution of cross kinks.

The temperature dependence of the stress in eq. (5) at a reference strain rate of 10^{-3} s^{-1} for the real alloy is given in Figure 8. The curves show a noticeable softening as T increases, starting with a value of 181 MPa at 300 K, down to a saturation level of

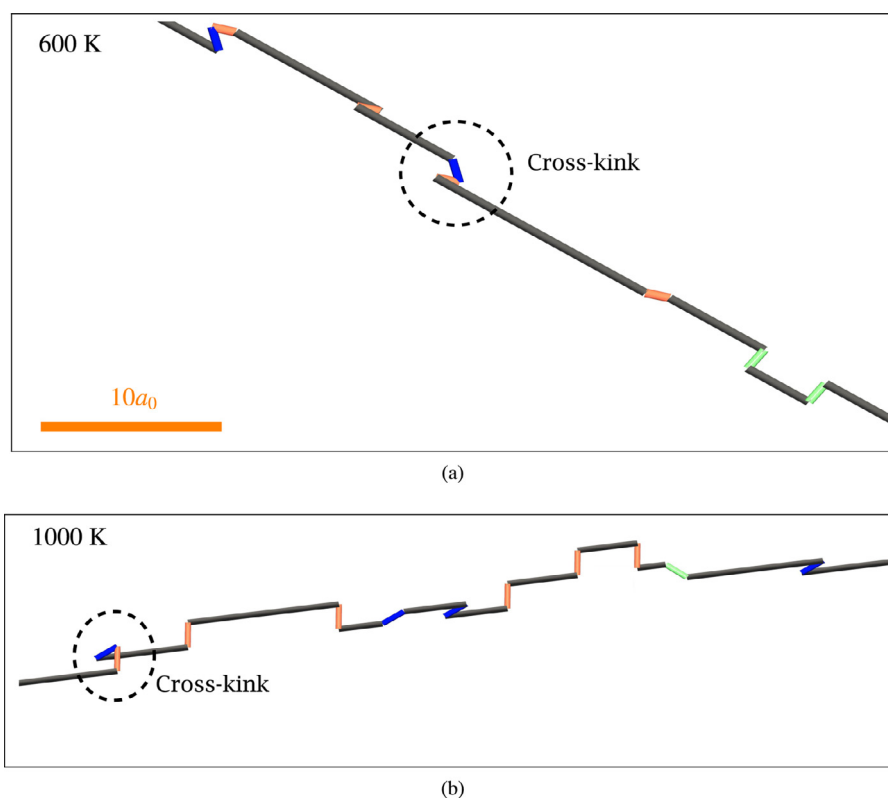


Fig. 6. Dislocation configurations after thermalization at (a) 1000 and, (b), 1500 K. Cross-kinks emerge spontaneously during the equilibration at both temperatures, as well as kink-pairs on several different slip planes (color-coded accordingly). The scale marker in (a) is common to both (a) and (b).

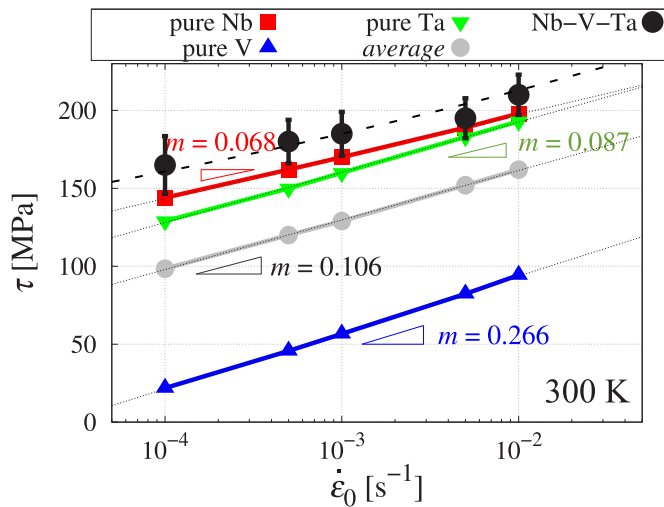


Fig. 7. Strain-rate dependence of the resolved stress at 300 K. Remarkably, the alloy strength exceeds that of Nb, the strongest of the individual alloy components. The associated strain-rate sensitivity exponents are shown next to each curve. $m = 0.06$ for the Nb-V-Ta alloy.

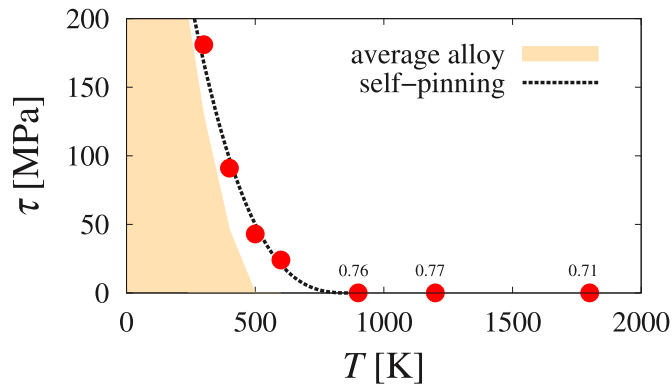


Fig. 8. Temperature dependence of the dislocation stress in the Nb-Ta-V alloy at a reference strain rate of 10^{-3} s^{-1} . The values in MPa at 900, 1200, and 1800 K are indicated in the figure.

approximately 0.7 MPa above 600 K. The shaded area in the figure represents the strength of the average alloy, while the dashed line corresponds to the expression:

$$\tau(T) = \tau_0(1 - cT)^n$$

where τ_0 , c , and n are fitting constants whose least-squares regression values are 550 MPa, 0.001 K^{-1} and 2.8, respectively.

While it is difficult to make a direct association between these parameters and actual physical constants, the above expression can be obtained by inverting a standard thermally-activated screw dislocation velocity function where τ_0 represents the Peierls stress [47]. Inspection of our simulations, however, suggests that the dynamic process taking place in the low temperature region is *self-pinning*, i.e., local formation of sessile locks on the dislocation line due to cross-kinks. Thus, τ_0 can be construed as the stress needed to overcome cross-kinks by creating debris loops (an illustrative animation is attached to this paper as *Supplementary Information*).

For its part, the athermal regime begins above 900 K, and is characterized by a constant value of $\tau_{\text{ath}} \approx 0.7 \sim 0.8$ MPa. Interestingly, the operating mechanism in this regime is the lateral migration of cross-kinks, leading to their dissolution (see attached animation in the *Supplementary Information*). The role played by each

of these mechanisms in the dislocation's stress response is analyzed in depth next.

3.3. Role of cross-kinks

The picture that emanates from Secs. 3.1 and 3.2 is that cross kinks control screw dislocation glide at low and intermediate temperatures. Without them, the intrinsic lattice resistance is nullified by chemical interactions between lattice atoms and screw dislocation cores. Consequently, the contribution of screw dislocations to the strength of the alloy is governed by the stress required to resolve (or 'dissolve') these cross kinks.

The resolution of cross kinks can occur via (i) interactions of several kinks on multiple complementary slip planes resulting in the formation of closed loops, or (ii) by cross kink diffusion along the dislocation line resulting in mutual annihilation³. Between 300 and 600 K, mechanism (i) is preferentially observed, which leads to a relatively high alloy strength. A visual example of self-pinning at 400 K and 10^{-3} s^{-1} is shown in Figure 9, where the process of formation of trailing prismatic loops is captured.

Above 600 K, however, cross kinks can also disappear by mutual annihilation. Figure 10 contains a sequence of simulation snapshots showing the cancellation of two oppositely-signed cross-kinks at 900 K and 10^{-3} s^{-1} . The sequence shows two cross-kinks moving laterally towards one another, driven by stress and temperature. Our simulations indicate that this process is more prevalent at temperatures of 900 K and above, when these cross-kink 'dipoles' are more common. This is hardly observed in pure metals, where the stress needed to move a cross kink is typically exceedingly high. In this mechanism, kink motion becomes the rate-limiting step, even though the required stresses are quite low [68].

The lateral motion of a cross-kink requires that one of the two kinks involved must move against the action of the applied stress. This of course negates the very strengthening effect by which cross-kinks are effective obstacles to further dislocation progression due to the opposing directions of their constituent kinks. However, our simulations demonstrate that at high temperatures this does indeed occur, facilitated by three main conflating factors: (i) the low applied stresses (~ 0.8 MPa), (ii) the elastic attraction between the two kinks in a cross-kink, and (iii) the spatial fluctuations of the energy landscape, which introduces opportunities for a kink to move against the applied stress direction. Factors (i) and (ii) can of course exist in pure metals (or dilute alloys), and thus the differentiating feature of this mechanism is (iii). Overall, the motion of these cross-kinks resembles a diffusive process in which cross-kinks fluctuate between forward and backward jumps, as shown in the animation provided in the *Supplementary Information*. While the stresses required are < 1 MPa, this mechanism confers the Nb-Ta-V alloy with some extra strength not existent in pure or dilute bcc alloys.

4. Discussion

4.1. Physical model

The underlying physical model in this study is based on past works [36,69] that assume that a multielement alloy can be decomposed into a substrate or matrix that possesses the average properties of its elementary constituents and on which every lattice atom constitutes a solute atom. Much in the manner of pure

³ Note that both of these mechanisms are *conservative*, i.e., no transport of matter is required to activate them. The possibility of cross-kink dragging along the glide direction due to non-conservative point defect diffusion exists (akin to jog-dragging in fcc crystals). Although this mechanism is not captured by our model, it is reasonable to presume that it is less likely than the other ones due to the large energies required.

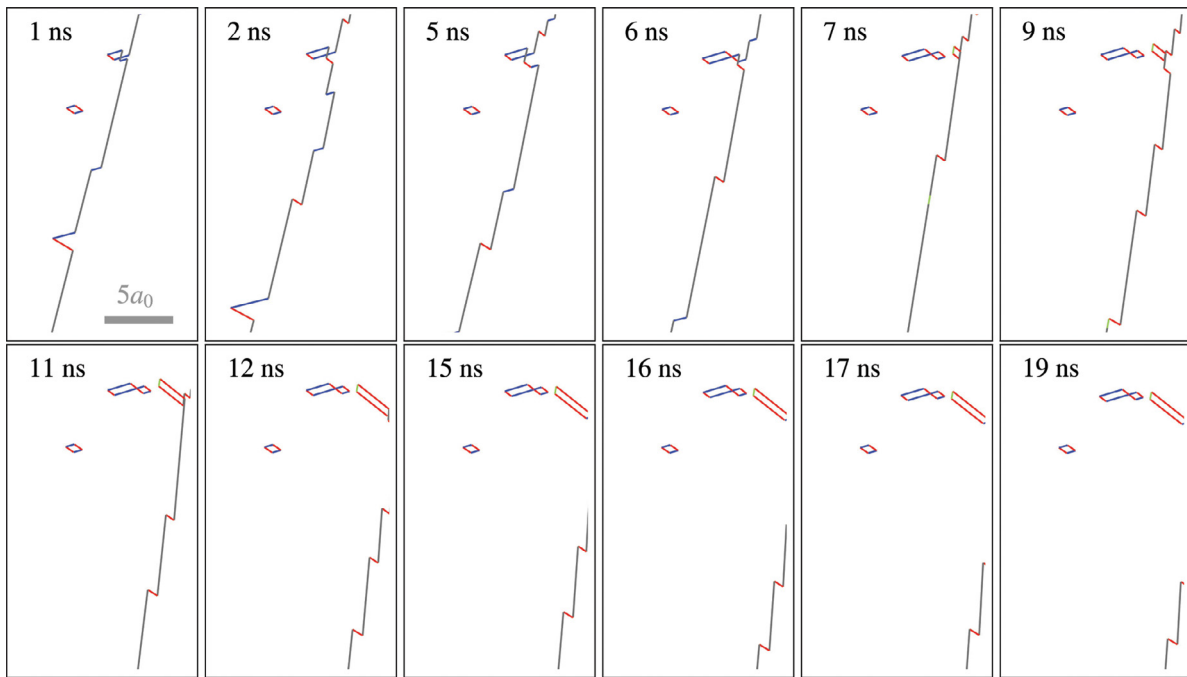


Fig. 9. Sequence of simulation snapshots showing the formation of closed loops from reactions among cross-kinks at 400 K and 10^{-3} s^{-1} . Different colors represent segments lying on different planes. Red-colored kinks lie on the MRSS plane. The scale marker provided in the first image is common to all snapshots. An animation showing excerpts of this behavior is provided as *Supplementary Information*.

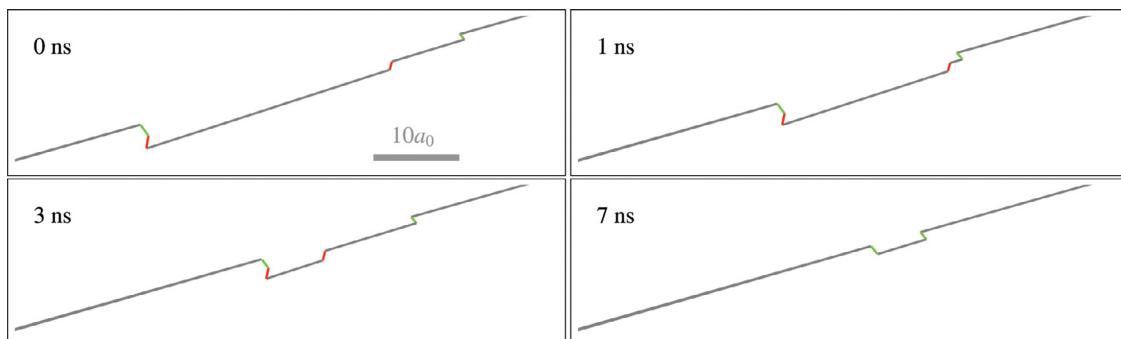


Fig. 10. Sequence of simulation snapshots showing the annihilation of two cross-kinks at 900 K and 10^{-3} s^{-1} . This occurs under stresses of approximately 0.7 MPa. The kinetic process includes a diffusional component, which makes kinks follow random walks along both directions of the dislocation line. Red-colored kinks lie on the MRSS plane. The scale marker provided is common to all images. An animation showing excerpts of this behavior is provided as *Supplementary Information*.

bcc metals, the ‘average’ alloy displays a relatively high kink-pair activation energy and a low resistance to single kink motion. However, the spatial complexity of compositional fluctuations in the true alloy affects the material in three principal ways:

1. The ground state of a dislocation line is characterized by an intrinsic roughness manifested by a high concentration of kink pairs coexisting at every given moment on multiple glide planes.
2. The *effective* kink-pair energy all but vanishes in the multielement alloy at low temperatures (0.02 eV) and is significantly reduced at higher T (0.20 eV).
3. Cross-kinks exist in significant (equilibrium) concentrations at temperatures above 600 K. These cross-kinks govern the subsequent dynamic behavior of the alloy during deformation.

All these effects confer a very particular nature to the Nb-Ta-V alloy that cannot be surmised from pure material properties. Indeed, looked through the lens of standard bcc behavior, a low ef-

fective kink-pair energy would be expected to result in a soft response at all temperatures (albeit this effect can be partially compensated by limiting kink mobility, e.g., via solute-kink interactions [47]), which is in opposition of what is observed here.

Spontaneous kink-pair nucleation make the alloy amenable to glide on multiple non-MRSS planes of the [111] zone [70,71], leading to an enhanced cross kink formation and self-pinning via debris loop formation. Ultimately, this self-pinning is behind the extra strength of these alloys at low temperature. Cross-kink-dominated kinetics is specific to long screw dislocations in bcc metals, and thus cannot be studied using small supercells with electronic structure methods. Molecular dynamics simulations of screw dislocations in bcc materials do capture cross-kink formation and closure. However, due to their overdriven⁴ nature, even at relatively low temperatures and stresses [45,64,72,73], it is dif-

⁴ This refers to the inability to sample thermally-activated processes on realistic time scales.

ficult to discern whether self-pinning due to cross kink kinetics is truly an intrinsic dynamic modality of screw dislocation glide or an artifact of the simulation conditions.

By contrast, our kMC model is designed to sample among all available processes in the dislocation with the correct probability. This allows us to (i) study dislocation kinetics as a sequence of non-overlapping events that accurately represent steady state, and (ii) access more realistic timescales than MD studies. Our simulations reveal a picture in which cross-kinks unequivocally govern dislocations' slip activity, leading to a marked temperature dependence of the alloy strength, characterized by self-pinning at low temperature and cross-kink diffusion and annihilation at high temperature. In summary, our results indicate that cross-kink dynamics is responsible for the cocktail effect in these systems, an observation that can only be accessed by simulating long dislocation lines gliding on multiple glide planes (currently beyond the capabilities of direct atomistic methods).

4.2. Discussion on model limitations and physical assumptions

As all kMC simulations, the present model is predicated on the *rare event* (i.e., *thermally-activated*) nature of a set of physical processes describing dislocation evolution. For this, the system follows a dynamic trajectory between a set of connected thermalized (equilibrated) states. Generally, it is accepted that physical processes characterized by deep energy wells separated by high energy barriers fit this classification. However, the minute kink-pair nucleation energies found in some cases in the true alloy lead to differences between adjacent states that can hardly qualify them as time-uncorrelated. This emphasizes the need to capture atomistic environments around the dislocation core that provide as much crystal detail as possible, to ensure an accurate calculation of interaction energies and transition rates. In any case, this problem of 'shallow barriers' does not in general invalidate the utility of kMC calculations, as has been noted and dealt with in the literature [68,74–76].

Another approximation worth mentioning is the manner in which single kink interaction energies are computed. Here we assume that the total interaction energy of a kink segment spread over a distance $a = 12b$ is determined by all the atoms in the chemical environment created around it (as shown in Fig. 2). However, in the current kMC implementation, the calculation of the interaction energy disregards the non-screw character of kinks, which is simply calculated in the same manner as for the kink-pair interaction energy. Moreover, we assume that changes in interaction energies during kink motion can be reduced to the difference between the energy of the next atomic slice entered by the kink in its motion (refer to Fig. 2(b)) and the slice left behind, i.e., the interaction energy difference is solely determined by the end slices of the kink atomic envelope. Detailed comparisons with theoretical and atomistic simulations will elucidate if this is a satisfactory approximation.

Finally, there are two points worth mentioning related to the alloy configurations in the crystal lattice. First, our method belongs to the general class of 'lattice' kinetic Monte Carlo methods. In the absence of atomic relaxations, our approach cannot furnish transition energy barriers, relying instead on equilibrium state energy differences and/or pre-computed barriers. As such, some of the transitions simulated here may yield a different time scale than predicted in our simulations. Ongoing molecular statics calculations of detailed compositionally-dependent transition energies will help us understand the importance of these limitations. Second, it has been noted that multicomponent alloys containing the elements Mo, Nb, Ta, V, W, i.e., of which ours can be considered a subset, display non-negligible short-range order (SRO) up to 1000 K [77,78]. SRO can be made to emerge from

crystal relaxation simulations by a number of different techniques such as, among others, Monte Carlo structural optimizations based on cluster-expansion Hamiltonians [77,79] or by generating *special quasirandom structures* subjected to configurational constraints [80,81]. Quantitatively, SRO adds a hardening component to dislocation glide due to lattice forces that opposes the destruction of local order due to slip [82,83]. At present, this effect is beyond the scope of this paper.

4.3. Significance of the results in the context of present research on refractory multi-element alloys

The evidence from numerous MD studies in several RMEA consistently points to a ground state of screw dislocations characterized by rough line shapes [35,62,64,84]. Such states are likely to be micro-states, i.e., reflective of the length scale over which compositional fluctuations take place, which is on the order of one atomic distance. Indeed, such roughness is not captured experimentally with conventional microscopy [71,85]. Our kMC model is able to capture this intrinsic roughness naturally from the underlying atomistic model, as shown in Figs. 5 and 6, with good qualitative agreement with atomistic configurations. This adds confidence to the approach in anticipation of the dynamic simulations.

What is clearly observed in experiments at room temperature is the telltale signature of self-pinning by cross-kink resolution, i.e. trailing debris formed in the wake of moving dislocations [85]. This is an encouraging sign in the direction of qualitative validation of theoretical models of RMEA strength. Cross-kink formation is favored by a number of different factors, of which spontaneous kink-pair formation is only one. Recent evidence of a screw dislocation core dissociation [81,84,86,87], in contrast with the compact cores displayed in pure bcc metals [50,51], also suggests enhanced pathways for the formation of kinks on non-MRSS planes. Our model naturally captures kink pair nucleation and glide on all 110-type planes of the [111] zone, as sampled from the activation rate determined by the applied shear stress from eq. (5). Thus, our simulations naturally enable the kinetics needed for cross-kink formation.

It is worth mentioning that, while our strain-rate-driven simulations correspond to lines with a length of $L = 500b$ (≈ 140 nm) –consistent with the value of ρ_d used here–, we have shown in past studies [39] that in the cross-kink dominated regime the dislocation velocity becomes length-independent. This suggests that, to the extent that the dislocation source length is determined by the forest dislocation density, the alloy strength at low temperature may be independent of the amount of strain hardening in these alloys. Future experiments may be able of proving or disproving such conjecture, but this shows how modeling and simulation can guide and motivate further experimental examination in RMEA.

4.4. Beyond a thermally activated model of screw dislocation motion in RMEA

Our results clearly indicate that screw dislocations are unlikely to be the source of the unusually-high strength in multi-element alloys at high temperature (specifically Nb-Ta-V in this case). It has been hypothesized that edge dislocations are responsible for the high temperature strength in RMEA [36]. It is well known that edge dislocations begin to contribute to a material's strength in a temperature range where their mobilities equalize with those of screw dislocations [88]. In pure bcc metals, phonon drag dampens edge dislocation mobility to the level of screw dislocations as the temperature increases [55,89]. In RMEA, additional

mechanisms exist that can contribute to this slowdown. More importantly, however, is that these mechanisms are not diminished by temperature in the same way that screw dislocation mobility is [36], so that they can take over when screw dislocations can no longer provide the level of strength displayed in these alloys.

Another alternative can yet be conceived from consideration of the low kink-pair energies obtained here. This may put screw dislocations directly in the phonon-drag region of the stress-velocity space at moderate and high temperatures [55], within which their behavior qualitatively resembles that of edge dislocations and where the kMC approach can no longer be used. Thus, the possibility of screw dislocations substantially contributing to the material's strength at high temperature should not be discounted. As always, further research is needed to explore these possibilities.

In all, our findings are but one piece in a complex puzzle needing to be solved to understand the mechanical behavior of RMEA. Similarly, the kMC method employed here –with all its advantages and limitations– should be regarded as one of many techniques, including of course experiments, that should be applied in conjunction to resolve the details of the response of these promising materials.

5. Conclusions

We finish with our main conclusions:

1. We have developed a kinetic Monte Carlo model of thermally activated screw dislocation kinetics in the equiatomic Nb-Ta-V alloy. The model includes an extensive atomistic envelope around the dislocation to calculate all the necessary interaction energies from the surrounding atomic configurations. These environments ensure that correlated transitions are properly accounted for, and that a statistically significant material volume is sampled.
2. The strength of the alloy due to screw dislocations decreases sharply with temperature, ranging from 181 MPa at 300 K to 0.8 MPa at and above 900 K.
3. At room temperature, the alloy is stronger than its individual pure constituents and than the 'average' alloy (obtained by averaging the material properties of Nb, Ta, and V). Its strain rate sensitivity exponent is $m = 0.06$.
4. Our simulations reveal a picture by which cross-kinks unequivocally govern screw dislocation activity, leading to a marked temperature dependence of the alloy strength. Alloy strength is characterized by self-pinning at low temperature and cross-kink diffusion and annihilation at high temperature.
5. The alloy strength remains unchanged above 900 K. This is consistent with a saturated (constant) kink diffusivity in that temperature range, which is characterized by rough dislocation lines with significant concentrations of cross kinks.

Declaration of Competing Interest

The authors declare that they have no known competing financial interests or personal relationships that could have appeared to influence the work reported in this paper.

Acknowledgements

This work has been funded by the National Science Foundation under Grant No. DMR-1611342. We thank UCLA's IDRE for computer time allocations on the Hoffman2 supercomputer. Helpful discussions with W. Curtin and F. Maresca are gratefully acknowledged.

Supplementary material

Supplementary material associated with this article can be found, in the online version, at doi:[10.1016/j.actamat.2021.116875](https://doi.org/10.1016/j.actamat.2021.116875)

References

- [1] B. Cantor, I. Chang, P. Knight, A. Vincent, Microstructural development in equiatomic multicomponent alloys, *Materials Science and Engineering: A* 375–377 (2004) 213–218, doi:[10.1016/j.msea.2003.10.257](https://doi.org/10.1016/j.msea.2003.10.257).
- [2] J.-W. Yeh, S.-K. Chen, S.-J. Lin, J.-Y. Gan, T.-S. Chiu, T.-T. Shun, C.-H. Tsau, S. Y. Chang, Nanostructured high-entropy alloys with multiple principal elements: Novel alloy design concepts and outcomes, *Advanced Engineering Materials* 6(5) 299–303. 10.1002/adem.200300567
- [3] L.S. Zhang, G.L. Ma, L.C. Fu, J.Y. Tian, Recent progress in high-entropy alloys, in: *Materials Engineering for Advanced Technologies (ICMEAT 2012)*, Vol. 631 of *Advanced Materials Research*, Trans Tech Publications Ltd, 2013, pp. 227–232. 10.4028/www.scientific.net/AMR.631-632.227
- [4] J.W. Yeh, Y.L. Chen, S.J. Lin, S.K. Chen, High-entropy alloys ? a new era of exploitation, in: *Advanced Structural Materials III*, Vol. 560 of *Materials Science Forum*, Trans Tech Publications Ltd, 2007, pp. 1–9. 10.4028/www.scientific.net/MSF.560.1
- [5] E.J. Pickering, N.G. Jones, High-entropy alloys: a critical assessment of their founding principles and future prospects, *International Materials Reviews* 61 (3) (2016) 183–202, doi:[10.1080/09506608.2016.1180020](https://doi.org/10.1080/09506608.2016.1180020).
- [6] M.C. Gao, J.-W. Yeh, P.K. Liaw, Y. Zhang, *High-Entropy Alloys*, Springer, Cham, 2016, doi:[10.1007/978-3-319-27013-5](https://doi.org/10.1007/978-3-319-27013-5).
- [7] D. Miracle, O. Senkov, A critical review of high entropy alloys and related concepts, *Acta Materialia* 122 (2017) 448–511, doi:[10.1016/j.actamat.2016.08.081](https://doi.org/10.1016/j.actamat.2016.08.081).
- [8] M.-H. Tsai, J.W. Yeh, High-entropy alloys: A critical review, *Materials Research Letters* 2 (3) (2014) 107–123, doi:[10.1080/21663831.2014.912690](https://doi.org/10.1080/21663831.2014.912690).
- [9] O.N. Senkov, D.B. Miracle, K.J. Chaput, J.P. Couzinie, Development and exploration of refractory high entropy alloys? a review, *Journal of Materials Research* 33 (19) (2018) 3092–3128, doi:[10.1557/jmr.2018.153](https://doi.org/10.1557/jmr.2018.153).
- [10] M.C. Gao, J. Qiao, High-entropy alloys (heas), *Metals* 8(2). 10.3390/met8020108
- [11] B. Gludovatz, A. Hohenwarter, D. Catoor, E.H. Chang, E.P. George, R.O. Ritchie, A fracture-resistant high-entropy alloy for cryogenic applications, *Science* 345 (6201) (2014) 1153–1158, doi:[10.1126/science.1254581](https://doi.org/10.1126/science.1254581).
- [12] S.-q. Xia, W. Zhen, T.-f. Yang, Y. Zhang, Irradiation behavior in high entropy alloys, *Journal of Iron and Steel Research, International* 22 (10) (2015) 879–884.
- [13] S. Xia, M.C. Gao, T. Yang, P.K. Liaw, Y. Zhang, Phase stability and microstructures of high entropy alloys ion irradiated to high doses, *Journal of Nuclear Materials* 480 (2016) 100–108.
- [14] N.K. Kumar, C. Li, K. Leonard, H. Bei, S. Zinkle, Microstructural stability and mechanical behavior of fcc high entropy alloy under ion irradiation, *Acta Materialia* 113 (2016) 230–244.
- [15] T. Egami, W. Guo, P. Rack, T. Nagase, Irradiation resistance of multicomponent alloys, *Metallurgical and Materials Transactions A* 45 (1) (2014) 180–183.
- [16] R. Kozak, A. Sologubenko, W. Steurer, Single-phase high-entropy alloys: an overview, *Zeitschrift für Kristallographie - Crystalline Materials* 230 (1) (2015) 55–68, doi:[10.1515/zkri-2014-1739](https://doi.org/10.1515/zkri-2014-1739).
- [17] High-entropy alloys: Formation and properties. Vol. ASME 2018 Symposium on Elevated Temperature Application of Materials for Fossil, Nuclear, and Petrochemical Industries of Pressure Technology, v001T01A004. 10.1115/ETAM2018-6732
- [18] O. Senkov, J. Miller, D. Miracle, C. Woodward, Accelerated exploration of multi-principal element alloys for structural applications, *Calphad* 50 (2015) 32–48.
- [19] D.B. Miracle, J.D. Miller, O.N. Senkov, C. Woodward, M.D. Uchic, J. Tiley, Exploration and development of high entropy alloys for structural applications, *Entropy* 16 (1) (2014) 494–525, doi:[10.3390/e16010494](https://doi.org/10.3390/e16010494).
- [20] Y. Zhang, T. Zuo, Z. Tang, M. Gao, K. Dahmen, P. Liaw, Z. Lu, Microstructures and properties of high-entropy alloys, *Progress in Materials Science* 61 (2014) 1–93, doi:[10.1016/j.pmatsci.2013.10.001](https://doi.org/10.1016/j.pmatsci.2013.10.001).
- [21] O. Senkov, G. Wilks, J. Scott, D. Miracle, Mechanical properties of $\text{Nb}_{25}\text{Mo}_{25}\text{Ta}_{25}\text{W}_{25}$ and $\text{V}_{20}\text{Nb}_{20}\text{Mo}_{20}\text{Ta}_{20}\text{W}_{20}$ refractory high entropy alloys, *Intermetallics* 19 (5) (2011) 698–706, doi:[10.1016/j.intermet.2011.01.004](https://doi.org/10.1016/j.intermet.2011.01.004).
- [22] Y. Zou, S. Maiti, W. Steurer, R. Spolenak, Size-dependent plasticity in an $\text{Nb}_{25}\text{Mo}_{25}\text{Ta}_{25}\text{W}_{25}$ refractory high-entropy alloy, *Acta Materialia* 65 (2014) 85–97, doi:[10.1016/j.actamat.2013.11.049](https://doi.org/10.1016/j.actamat.2013.11.049).
- [23] H. Yao, J.-W. Qiao, M.C. Gao, J.A. Hawk, S.-G. Ma, H. Zhou, Monobitav medium-entropy alloy, *Entropy* 18(5). 10.3390/e18050189
- [24] F. Körmann, M.H. Sluiter, Interplay between lattice distortions, vibrations and phase stability in nbmotaw high entropy alloys, *Entropy* 18(8). 10.3390/e18080403
- [25] H. Yao, J. Qiao, J. Hawk, H. Zhou, M. Chen, M. Gao, Mechanical properties of refractory high-entropy alloys: Experiments and modeling, *Journal of Alloys and Compounds* 696 (2017) 1139–1150, doi:[10.1016/j.jallcom.2016.11.188](https://doi.org/10.1016/j.jallcom.2016.11.188).
- [26] H. Dobbelsstein, M. Thiele, E.L. Gurevich, E.P. George, A. Ostendorf, Direct metal deposition of refractory high entropy alloy monobitav, *Physics Procedia* 83 (2016) 624–633, doi:[10.1016/j.phpro.2016.08.065](https://doi.org/10.1016/j.phpro.2016.08.065). Laser Assisted Net Shape Engineering 9 International Conference on Photonic Technologies Proceedings of the LANE 2016 September 19–22, 2016 F7rth, Germany
- [27] S.A. Kube, S. Sohn, D. Uhl, A. Datye, A. Mehta, J. Schroers, Phase selection motifs in high entropy alloys revealed through combinatorial methods: Large

- atomic size difference favors bcc over fcc, *Acta Materialia* 166 (2019) 677–686, doi:10.1016/j.actamat.2019.01.023.
- [28] S.-Y. Chang, C.-E. Li, Y.-C. Huang, H.-F. Hsu, J.-W. Yeh, S.J. Lin, Structural and thermodynamic factors of suppressed interdiffusion kinetics in multi-component high-entropy materials, *Scientific Reports* 4 (1) (2014) 4162.
- [29] D. Beke, G. Erdaglyi, On the diffusion in high-entropy alloys, *Materials Letters* 164. 10.1016/j.matlet.2015.09.028
- [30] S. Zhao, Y. Osetskyy, Y. Zhang, Preferential diffusion in concentrated solid solution alloys: NiFe, NiCo and NiCoCr, *Acta Materialia* 128 (2017) 391–399, doi:10.1016/j.actamat.2017.01.056.
- [31] A. Roy, J. Munshi, G. Balasubramanian, Low energy atomic traps sluggish the diffusion in compositionally complex refractory alloys, *Intermetallics* 131 (2021) 107106, doi:10.1016/j.intermet.2021.107106.
- [32] V. Soni, O.N. Senkov, B. Gwalani, D.B. Miracle, R. Banerjee, Microstructural design for improving ductility of an initially brittle refractory high entropy alloy, *Scientific Reports* 8 (1) (2018) 8816, doi:10.1038/s41598-018-27144-3.
- [33] J.-W. Yeh, S.J. Lin, Breakthrough applications of high-entropy materials, *Journal of Materials Research* 33 (19) (2018) 3129–3137, doi:10.1557/jmr.2018.283.
- [34] S. Rao, E. Antillon, C. Woodward, B. Akdim, T. Parthasarathy, O. Senkov, Solution hardening in body-centered cubic quaternary alloys interpreted using Suzuki's kink-solute interaction model, *Scripta Materialia* 165 (2019) 103–106.
- [35] F. Maresca, W.A. Curtin, Theory of screw dislocation strengthening in random bcc alloys from dilute to "high-entropy" alloys, *Acta Materialia* 182 (2020) 144–162.
- [36] F. Maresca, W.A. Curtin, Mechanistic origin of high strength in refractory bcc high entropy alloys up to 1900K, *Acta Materialia* 182 (2020) 235–249.
- [37] B. Yin, W. Curtin, Origin of high strength in the CoCrFeNiPd high-entropy alloy, *Materials Research Letters* 8 (6) (2020) 209–215.
- [38] M.R. Gilbert, S. Queyreau, J. Marian, Stress and temperature dependence of screw dislocation mobility in α -Fe by molecular dynamics, *Phys. Rev. B* 84 (2011) 174103, doi:10.1103/PhysRevB.84.174103.
- [39] A. Stukowski, D. Cereceda, T.D. Swinburne, J. Marian, Thermally-activated non-schmid glide of screw dislocations in w using atomistically-informed kinetic monte carlo simulations, *International Journal of Plasticity* 65 (2015) 108–130, doi:10.1016/j.ijplas.2014.08.015.
- [40] D. Cereceda, M. Diehl, F. Roters, D. Raabe, J.M. Perlado, J. Marian, Unraveling the temperature dependence of the yield strength in single-crystal tungsten using atomistically-informed crystal plasticity calculations, *International Journal of Plasticity* 78 (2016) 242–265, doi:10.1016/j.ijplas.2015.09.002.
- [41] L.L. Hsiung, On the mechanism of anomalous slip in bcc metals, *Materials Science and Engineering: A* 528 (1) (2010) 329–337.
- [42] C.R. Weinberger, B.L. Boyce, C.C. Battaile, Slip planes in bcc transition metals, *International Materials Reviews* 58 (5) (2013) 296–314.
- [43] M. Hossain, J. Marian, Stress-dependent solute energetics in wre alloys from first-principles calculations, *Acta Materialia* 80 (2014) 107–117, doi:10.1016/j.actamat.2014.07.028.
- [44] Y. Zhao, L. Dezerald, J. Marian, Electronic structure calculations of oxygen atom transport energetics in the presence of screw dislocations in tungsten, *Metals* 9 (2) (2019) 252.
- [45] J. Marian, W. Cai, V.V. Bulatov, Dynamic transitions from smooth to rough to twinning in dislocation motion, *Nature materials* 3 (3) (2004) 158.
- [46] A. Stukowski, D. Cereceda, T.D. Swinburne, J. Marian, Thermally-activated non-schmid glide of screw dislocations in w using atomistically-informed kinetic monte carlo simulations, *International Journal of Plasticity* 65 (2015) 108–130.
- [47] Y. Zhao, J. Marian, Direct prediction of the solute softening-to-hardening transition in w-re alloys using stochastic simulations of screw dislocation motion, *Modelling and Simulation in Materials Science and Engineering* 26 (4) (2018) 045002, doi:10.1088/1361-651x/aaacfc.
- [48] Y. Zhao, L. Dezerald, M. Pozuelo, X. Zhou, J. Marian, Simulating the mechanisms of serrated flow in interstitial alloys with atomic resolution over diffusive timescales, *Nature Communications* 11 (1) (2020) 1–8.
- [49] A. Ghafarollahi, F. Maresca, W. Curtin, Solute/screw dislocation interaction energy parameter for strengthening in bcc dilute to high entropy alloys, *Modelling and Simulation in Materials Science and Engineering* 27 (8) (2019) 085011.
- [50] C.R. Weinberger, G.J. Tucker, S.M. Foiles, Peierls potential of screw dislocations in bcc transition metals: Predictions from density functional theory, *Phys. Rev. B* 87 (2013) 054114, doi:10.1103/PhysRevB.87.054114.
- [51] L. Dezerald, L. Provaille, L. Ventelon, F. Willaime, D. Rodney, First-principles prediction of kink-pair activation enthalpy on screw dislocations in bcc transition metals: V, Nb, Ta, Mo, W, and Fe, *Phys. Rev. B* 91 (2015) 094105, doi:10.1103/PhysRevB.91.094105.
- [52] W. Cai, V.V. Bulatov, S. Yip, A.S. Argon, Kinetic monte carlo modeling of dislocation motion in bcc metals, *Materials Science and Engineering: A* 309 (2001) 270–273.
- [53] S. Shinzato, M. Wakeda, S. Ogata, An atomistically informed kinetic monte carlo model for predicting solid solution strengthening of body-centered cubic alloys, *International Journal of Plasticity* 122 (2019) 319–337.
- [54] U. Kocks, A. Argon, M. Ashby, Progress in materials science, *Thermodyn. Kinet. Slip* 19(11).
- [55] G. Po, Y. Cui, D. Rivera, D. Cereceda, T.D. Swinburne, J. Marian, N. Ghoniem, A phenomenological dislocation mobility law for bcc metals, *Acta Materialia* 119 (2016) 123–135.
- [56] X.W. Zhou, R.A. Johnson, H.N.G. Wadley, Misfit-energy-increasing dislocations in vapor-deposited CoFe/NiFe multilayers, *Phys. Rev. B* 69 (2004) 144113, doi:10.1103/PhysRevB.69.144113.
- [57] W. Cai, A. Arsenlis, C.R. Weinberger, V.V. Bulatov, A non-singular continuum theory of dislocations, *Journal of the Mechanics and Physics of Solids* 54 (3) (2006) 561–587, doi:10.1016/j.jmps.2005.09.005.
- [58] S. Aubry, A. Arsenlis, Use of spherical harmonics for dislocation dynamics in anisotropic elastic media, *Modelling and Simulation in Materials Science and Engineering* 21 (6) (2013) 065013, doi:10.1088/0965-0393/21/6/065013.
- [59] C.R. Weinberger, G.J. Tucker, S.M. Foiles, Peierls potential of screw dislocations in bcc transition metals: Predictions from density functional theory, *Physical Review B* 87 (5) (2013) 054114.
- [60] L. Dezerald, L. Provaille, L. Ventelon, F. Willaime, D. Rodney, First-principles prediction of kink-pair activation enthalpy on screw dislocations in bcc transition metals: V, Nb, Ta, Mo, W, and Fe, *Physical Review B* 91 (9) (2015) 094105.
- [61] S. He, E. Overly, V. Bulatov, J. Marian, D. Cereceda, Coupling 2d atomistic information to 3d kink-pair enthalpy models of screw dislocations in bcc metals, *Physical Review Materials* 3 (10) (2019) 103603.
- [62] S. Rao, C. Varvenne, C. Woodward, T. Parthasarathy, D. Miracle, O. Senkov, W. Curtin, Atomistic simulations of dislocations in a model bcc multicomponent concentrated solid solution alloy, *Acta Materialia* 125 (2017) 311–320.
- [63] S. Rao, C. Woodward, B. Akdim, E. Antillon, T. Parthasarathy, O. Senkov, Estimation of diffusional effects on solution hardening at high temperatures in single phase compositionally complex body centered cubic alloys, *Scripta Materialia* 172 (2019) 135–137.
- [64] B. Chen, S. Li, H. Zong, X. Ding, J. Sun, E. Ma, Unusual activated processes controlling dislocation motion in body-centered-cubic high-entropy alloys, *Proceedings of the National Academy of Sciences* 117 (28) (2020) 16199–16206.
- [65] S. Rao, C. Woodward, B. Akdim, O. Senkov, A model for interstitial solid solution strengthening of body centered cubic metals, *Materialia* 9 (2020) 100611.
- [66] K. Biswas, J.-W. Yeh, P.P. Bhattacharjee, J.T.M. DeHosson, High entropy alloys: Key issues under passionate debate, *Scripta Materialia* 188 (2020) 54–58.
- [67] J.W. Yeh, Physical metallurgy of high-entropy alloys, *Jom* 67 (10) (2015) 2254–2261.
- [68] T. Swinburne, S. Dudarev, S. Fitzgerald, M. Gilbert, A. Sutton, Theory and simulation of the diffusion of kinks on dislocations in bcc metals, *Physical Review B* 87 (6) (2013) 064108.
- [69] C. Varvenne, A. Luque, W.A. Curtin, Theory of strengthening in fcc high entropy alloys, *Acta Materialia* 118 (13) (2016) 164–176, doi:10.1016/j.actamat.2016.07.040.
- [70] E. Ma, X. Wu, Tailoring heterogeneities in high-entropy alloys to promote strength–ductility synergy, *Nature Communications* 10 (1) (2019) 5623.
- [71] F. Wang, G.H. Balbus, S. Xu, Y. Su, J. Shin, P.F. Rottmann, K.E. Knipling, J.-C. Stinville, L.H. Mills, O.N. Senkov, et al., Multiplicity of dislocation pathways in a refractory multiprincipal element alloy, *Science* 370 (6512) (2020) 95–101.
- [72] J. Chausson, M. Fivel, D. Rodney, The glide of screw dislocations in bcc Fe: atomistic static and dynamic simulations, *Acta materialia* 54 (13) (2006) 3407–3416.
- [73] H.-J. Lee, B.D. Wirth, Molecular dynamics simulation of dislocation–void interactions in bcc mo, *Journal of Nuclear Materials* 386 (2009) 115–118.
- [74] J. Rogal, K. Reuter, M. Scheffler, Co oxidation on Pd (100) at technologically relevant pressure conditions: First-principles kinetic monte carlo study, *Physical Review B* 77 (15) (2008) 155410.
- [75] G. Hupin, D. Lacroix, Quantum monte carlo method applied to non-markovian barrier transmission, *Physical Review C* 81 (1) (2010) 014609.
- [76] D. Chiarugi, M. Falaschi, D. Hermith, C. Olarte, L. Torella, Modelling non-markovian dynamics in biochemical reactions, *BMC systems biology* 9 (S3) (2015), S8
- [77] A. Fernández-Caballero, J.S. Wróbel, P.M. Mummery, D. Nguyen-Manh, Short-range order in high entropy alloys: Theoretical formulation and application to Mo-Nb-Ta-V-W system, *Journal of Phase Equilibria and Diffusion* 38 (4) (2017) 391–403.
- [78] S.W. McAlpine, J.V. Logan, M.P. Short, Predicting single phase stability and segregation in the NbMoTaTi–(W, V) high entropy alloy system with the vacancy exchange potential, *Scripta Materialia* 191 (2021) 29–33.
- [79] C.-H. Huang, L. Gharaee, Y. Zhao, P. Erhart, J. Marian, Mechanism of nucleation and incipient growth of re clusters in irradiated w-re alloys from kinetic monte carlo simulations, *Physical Review B* 96 (9) (2017) 094108.
- [80] A.V. de Walle, P. Tiwary, M. De Jong, D. Olmsted, M. Asta, A. Dick, D. Shin, Y. Wang, L.-Q. Chen, Z.K. Liu, Efficient stochastic generation of special quasirandom structures, *Calphad* 42 (2013) 13–18.
- [81] S. Yin, J. Ding, M. Asta, R.O. Ritchie, Ab initio modeling of the energy landscape for screw dislocations in body-centered cubic high-entropy alloys, *npj Computational Materials* 6 (1) (2020) 1–11.
- [82] J. Cohen, M. Fine, Some aspects of short-range order, *J. Phys. Radium* 23 (10) (1962) 749–762.
- [83] E.V. Kozlov, L.E. Popov, A.E. Ginzburg, Dislocation retardation due to the destruction of short-range order in the 112 superstructure, *Soviet Physics Journal* 14 (4) (1971) 486–491.
- [84] S. Rao, B. Akdim, E. Antillon, C. Woodward, T. Parthasarathy, O. Senkov, Modeling solution hardening in bcc refractory complex concentrated alloys: NbTiZr, NbTiZr_{0.5}Nb_{0.5}TiZr_{1.5}, *Acta Materialia* 168 (2019) 222–236.
- [85] L. Liliensten, J.-P. Couzini, L. Perrière, A. Hocini, C. Keller, G. Dirras, I. Guillot, Study of a bcc multi-principal element alloy: Tensile and simple shear proper-

- ties and underlying deformation mechanisms, *Acta Materialia* 142 (2018) 131–141, doi:10.1016/j.actamat.2017.09.062.
- [86] G.D. Samolyuk, Y. Osetsky, R. Stoller, The influence of transition metal solutes on the dislocation core structure and values of the peierls stress and barrier in tungsten, *Journal of Physics: Condensed Matter* 25 (2) (2012) 025403.
- [87] D. Cereceda, A. Stukowski, M. Gilbert, S. Queyreau, L. Ventelon, M.-C. Marinica, J. Perlado, J. Marian, Assessment of interatomic potentials for atomistic analysis of static and dynamic properties of screw dislocations in w, *Journal of Physics: Condensed Matter* 25 (8) (2013) 085702.
- [88] M. Tang, J. Marian, Temperature and high strain rate dependence of tensile deformation behavior in single-crystal iron from dislocation dynamics simulations, *Acta Materialia* 70 (2014) 123–129, doi:10.1016/j.actamat.2014.02.013.
- [89] S. Queyreau, J. Marian, M. Gilbert, B. Wirth, Edge dislocation mobilities in bcc fe obtained by molecular dynamics, *Physical Review B* 84 (6) (2011) 064106.